ACS OMEGA

Open Access

http://pubs.acs.org/journal/acsodf

Article

Analysis of Chemical Changes during Maturation of *Amomum tsao-ko* Based on GC-MS, FT-NIR, and FT-MIR

Gang He, Shao-bing Yang,* and Yuan-zhong Wang*

Cite This: *ACS Omega* 2024, 9, 29857−29869

Read Online

ACCESS | Metrics & More | Article Recommendations | Supporting Information

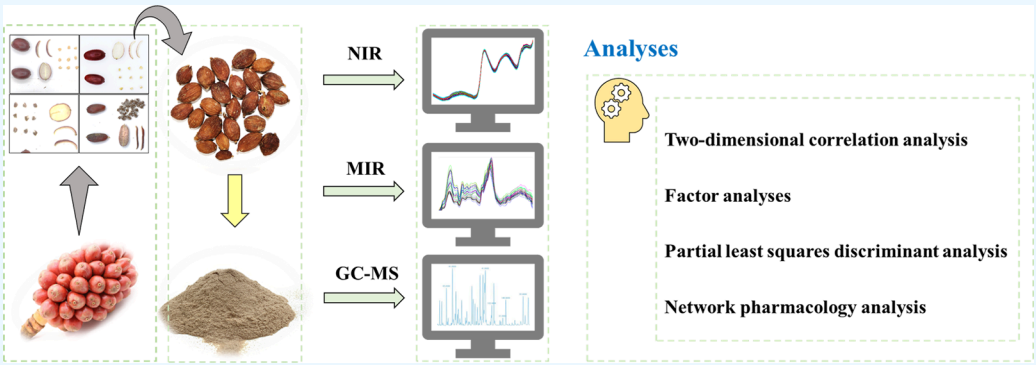

ABSTRACT: *Amomum tsao-ko* Crevost et Lemaire (*A. tsao-ko*) is widely grown for its high nutritional and economic value. However, the lack of a scientific harvesting and quality control system has resulted in an uneven product quality. The present study was based on *A. tsao-ko* from four maturity stages from the same growing area, and its chemical trends and quality were evaluated using a combination of agronomic trait analysis, spectroscopy, chromatography, chemometrics, and network pharmacology. The results showed that *A. tsao-ko* was phenotypically dominant in October. Spectroscopy showed that the absorbance intensity at different maturity stages showed a trend of October > September > August > July. Further chemical differences between *A. tsao-ko* at different stages of maturity were found by chromatography to originate mainly from alcohol, aromatic, acids, esters, hydrocarbons, ketone, heterocyclic, and aldehydes. The network pharmacology results showed that the active ingredient for the treatment of obesity was present in *A. tsao-ko* and had high levels in *A. tsao-ko* in September and October. The results of this study provide a new idea for the comprehensive evaluation of *A. tsao-ko* and a theoretical basis for the harvesting and resource utilization of *A. tsao-ko*.

1. INTRODUCTION

Epidemiological studies have shown that medicinal plants rich in natural products can help prevent or treat chronic diseases, and the research idea of "medicine and food from the same source" has been an important trend in the development of human health.[1] *Amomum tsao-ko* Crevost et Lemaire (*A. tsao-ko*) is a member of the cardamom genus of the ginger family, also known as black cardamom. It is a well-known traditional Southeast Asian spice, often used to flavor and deodorize beef and lamb during the cooking process.[2] It is also an important medicinal plant and is used in folklore to treat malaria, indigestion, diarrhea, and other ailments.[3] In southwest China, *A. tsao-ko* is also used as an important cash crop and is known as "Jin-guoguo", which means a fruit as valuable as gold. In recent years, with the increasing prevalence of metabolic syndrome diseases such as diabetes, hyperlipidemia and obesity, *A. tsao-ko* has a large application market in China due to its beneficial health properties.[4,5]

The harvesting of medicinal plants is time-specific. Plants whose seeds or fruits are used for medicinal purposes are harvested at or near natural maturity. In southwestern China, *A. tsao-ko* is more widely planted, but lacks a systematic management system, the quality of each planting area varies greatly, the harvest time is uncertain, and even the phenomenon that the harvest time of the same planting area is different every year.[2,6] The months of September and October are the main times for harvesting. As a result, there is also a large variation in the quality of *A. tsao-ko* circulating in the market. Different producers have different harvesting times, resulting in large fluctuations in the quality of *A. tsao-ko* from different growing regions, which may affect its efficacy. At present, there is no report on the chemical change trend of *A. tsao-ko* at maturity. Therefore, a comprehensive evaluation of the quality of *A. tsao-ko* at different stages of maturity is of

Received: April 17, 2024
Revised: June 5, 2024
Accepted: June 7, 2024
Published: June 24, 2024

https://doi.org/10.1021/acsomega.4c03717
ACS Omega 2024, 9, 29857−29869

Table 1. Measurements of Agronomic Characteristics of *A. tsao-ko* Fruits[a]

Traits	July	August	September	October
X_1 (mm)	38.55 ± 1.86	37.86 ± 1.26	41.41 ± 1.61	39.39 ± 2.02
X_2 (mm)	24.45 ± 1.36	25.4 ± 2.43	24.33 ± 0.67	26.52 ± 1.37
X_3 (g)	11.15 ± 1.43	11.18 ± 0.66	11.40 ± 0.56	14.20 ± 2.14
X_4 (mm)	2.37 ± 0.29	2.55 ± 0.32	2.12 ± 0.16	2.63 ± 0.24
X_5 (g)	5.12 ± 0.89	5.29 ± 0.42	5.39 ± 0.39	7.70 ± 0.90
X_6 (g)	3.66 ± 0.49	4.33 ± 0.20	4.70 ± 0.21	5.07 ± 0.88
X_7 (number)	38.00 ± 3.10	37.3 ± 2.05	35.40 ± 2.50	46.90 ± 6.98
X_8 (mm)	5.05 ± 0.49	5.67 ± 0.57	5.77 ± 0.60	4.70 ± 0.43
X_9 (mm)	7.06 ± 0.59	6.88 ± 0.50	6.49 ± 0.58	6.37 ± 0.52

[a]Note: X_1 = length of fruit; X_2 = width of fruit; X_3 = weight of fruit; X_4 = thickness of peel; X_5 = weight of peel; X_6 = weight of seeds; X_7 = number of seeds; X_8 = transverse diameter of seed; X_9 = longitudinal diameter of seeds.

interest, and the search for a fast, convenient, and accurate method for characterizing and analyzing chemical information is an important need for the industry. In Yunnan Province, the planting area of *A. tsao-ko* has exceeded 2.2 million acres, but the lack of scientific planting methods has resulted in low yields in most planting areas.[6] Varietal improvement and scientific and efficient cultivation may be important ways to increase yields.[7] Therefore, in the present study, in order to explore a comprehensive analytical approach for the harvesting of *A. tsao-ko*, phenotypic and chemical analyses of *A. tsao-ko* at different stages of maturity were performed.

Agronomic trait analysis can be based on the morphological characteristics of agricultural products to obtain whether there is an advantage in the growth of the species, in the same planting area, with growth advantage is an important basis for the selection of good seeds.[8] Based on this idea, this study applied agronomic traits to the comprehensive evaluation of *A. tsao-ko* at different stages of maturity, which can be judged from the dominance of external morphological characteristics. Based on the principle of genotype similarity, factor analysis is often used to comprehensively evaluate the relationship between agronomic traits, and can test and correlate subtle trait information.[9] In addition, variable projection importance analysis values (VIP) allows quantification of variables to compare the importance ranking of each agronomic trait.[10]

Chemical analysis is an important method for crop quality evaluation, and common methods include spectroscopic and chromatographic analysis.[11,12] Spectrometry is widely used in the characterization of comprehensive chemical information, classification and identification, and content prediction of agricultural products because of its rapidity, convenience and accuracy.[13,14] With the wide application of two-dimensional correlation spectroscopy (2DCOS), the ability of spectroscopy to characterize information has been strengthened, and it is capable of obtaining information on interactions within and between molecules, which is conducive to the comprehensive analysis and evaluation of chemical information.[15] Gas chromatography−mass spectrometry (GC-MS) is capable of detecting important chemical components and their relative contents in *A. tsao-ko*, and in conjunction with spectroscopic and chemometric methods, it can be used to make a preliminary determination of chemical variability in different species of genus *Amomum*, and is commonly used for the characterization of metabolic phenotypes.[13,16] In addition, the use of network pharmacology to predict the medicinal and nutritional values of species based on the results of GC-MS is also an important way to evaluate the quality of crops.[17]

In this work, nine agronomic traits such as length of fruit, weight of fruit, etc. were determined based on the observed phenotypic differences in *A. tsao-ko* at different maturity stages (July, August, September, and October) and were combined with factor analysis and partial least-squares discriminant analysis (PLS-DA) for obtaining the optimum maturity stage and important traits for discriminating between different maturity stages. The results were analyzed by factor analysis and partial least-squares discriminant analysis (PLS-DA). Meanwhile, Fourier transform near-infrared spectroscopy (FT-NIR), Fourier transform infrared spectroscopy (FT-MIR), GC-MS combined with chemometrics analysis, two-dimensional correlation analysis, and network pharmacology analysis were used to further explore the chemical change trends of *A. tsao-ko* at different maturity stages, predict the medicinal and health potential of *A. tsao-ko* for the treatment of obesity, screen out the important active factors, and determine the optimal harvesting period based on the relative content of the active factors in *A. tsao-ko* at different maturity stages. This study lays a theoretical foundation for the harvesting and comprehensive development of *A. tsao-ko* and provides new ideas for the quality evaluation of *A. tsao-ko*.

2. MATERIALS AND METHODS

2.1. Plant Materials. A total of four batches of *A. tsao-ko* were collected from Nujiang prefecture, Yunnan province, in different months. Samples were collected on the 25th day of each month and 5 kg of samples were collected each time (Figure S1). The samples collected in different months were from the same origin (Maji Township, Fugong County) and the distance between plants was not more than 20 m to reduce the interference caused by environmental factors (precipitation, soil, and temperature) and human factors (amount of fertilizer applied) to the experiment. Then, 10 samples were selected from all the samples of each month separately by random selection method, washed, and then dried to constant weight in an electrically heated thermostatic drying oven at 50 °C. The dried samples are pulverized using pulverizing equipment, passed through a 100 mesh sieve, and stored in a sealed bag protected from light for subsequent analysis and testing.

2.2. Determination of Agronomic Qualities. Before drying *A. tsao-ko* fruits, nine corresponding agronomic characters were measured including length of fruit (X_1), width of fruit (X_2), weight of fruit (X_3), thickness of peel (X_4), weight of peel (X_5), weight of seeds (X_6), number of seeds (X_7), transverse diameter of the seed (X_8), and longitudinal diameter of seeds (X_9). In this work, vernier calipers were used

https://doi.org/10.1021/acsomega.4c03717
ACS Omega 2024, 9, 29857−29869

for length measurements, and analytical balance was used for weight measurements; the results are shown in Table 1.

2.3. Spectra Analysis. *2.3.1. FT-NIR Spectra Acquisition.* Before the start of the experiment, the temperature of the laboratory was controlled to 25 °C and the humidity to 35% HR to ensure the stability of the apparatus and reduce the experimental error. In this study, an Antaris II spectrometer equipped with an integrating sphere was used, and after the warm-up of the equipment was completed, the instrument was adjusted to the diffuse reflectance mode, with the resolution set to 4 cm^{-1}, the scanning range of 10,000−4,000 cm^{-1}, and the number of scans to 64 cm^{-1}. After all the parameters were set, the spectral information on the background was collected (with the purpose of eliminating the interference of CO_2 and H_2O), after which the prepared sample powder was evenly spread on the bottom of the sample cup and the spectral information was started to be collected three times for each sample, and the average spectra were calculated for the subsequent analysis.

2.3.2. FT-MIR Spectra Acquisition. An FTIR spectrometer (Frontier PerkinElmer, USA) equipped with a diamond crystal attenuated total reflection accessory and a deuterated triglycine sulfate (DTGS) detector was used for spectral data acquisition of *A. tsao-ko* samples in the same laboratory environment as in 2.3.1. The experimental parameters for this work were: a scanning range of 4000−400 cm^{-1}, a resolution of 16 cm^{-1}, and 64 scans. Before each scan, background spectral information was collected, subtracting the background peaks of CO_2 and H_2O. Then, 0.5 g of the sample powder was weighed, and the powder was fixed on the diamond crystals using a solid press bar until the powder was pressed into a flake state. Then the acquisition of absorption spectrum information was started and repeated three times to calculate the average spectrum.

2.4. GC−MS Inspection. In this work, metabolite extraction and GC-MS analysis were performed using methods previously reported by the subject group.[13] From the 10 samples from each month, the first three samples were selected for analysis by GC-MS detection. Solid-phase microextraction (SPME) conditions were set as described in Table S1, and 0.5 g of each sample was used to extract volatile components. A Shimadzu Agilent 7890B gas chromatograph coupled to a LECO Pegasus BT mass spectrometer was used to perform the GC-MS analysis. The system is equipped with a DB-wax capillary column (30m × 0.25 mm × 0.25 μm) for chromatographic separation. Helium at a flow rate of 1 mL/min was used as the carrier gas for the separation of the derivatives. The initial temperature of the chromatographic column was 40 °C for 5 min. It then rises to 220 °C at a rate of 5 °C/min and then to 250 °C at a rate of 20 °C/min, holding for 2.5 min. The temperatures of injection, Ion source, and Quadrupole were 260 °C, 230 °C, and 150 °C, respectively. The mass selective detector (MSD) was run at 70 eV with an electron impact ion source; MS data were obtained by Full Scan, m/z in the range of 20−400.

2.5. Two-Dimensional Correlation Analysis. Generalized 2DCOS is an effective technique for improving spectral identification capabilities by designing disturbances (temperature, concentration, time) that cause dynamic changes in spectral signals.[18] Currently, generalized 2DCOS is divided into synchronous, asynchronous, and integrative images. Based on previous research results, synchronous 2DCOS images are more suitable for characterizing and analyzing the complex chemical systems of medicinal plants.[19,20] In this study, based on the FT-NIR and FT-MIR spectra of *A. tsao-ko* harvested in different months, synchronous 2DCOS images were further acquired based on Noda to improve the visual resolution of the spectra and to identify and analyze the chemical information on the overlapping characteristic peaks.[21] The correlation equations are shown in eqs 1 and 2, where P denotes the dynamic spectral intensity at variable v, t denotes the interval between external perturbations, and $\boldsymbol{\varphi}$ (v_m,v_m) denotes the synchronous two-dimensional correlation intensity between variables v_m and v_m.[10]

$$P(v) = \begin{cases} p(v_1, t_1) \\ p(v_2, t_2) \\ \vdots \\ p(v_m, t_m) \end{cases} \tag{1}$$

$$\boldsymbol{\varphi}(v_1, v_2) = \frac{1}{m-1} P(v_1)^T \cdot P(v_2) \tag{2}$$

In this study, there are two data sets converted into synchronous 2DCOS images, with a total of 80 2DCOS images obtained, and one is FT-NIR spectral data with a spectral range of 10,000−4,000 cm^{-1}, with a total of 1,557 variables. The other is FT-MIR spectral data with a spectral range of 4000−400 cm^{-1} and a total of 1868 variables. In this study, 2DCOS images were automatically generated using Matlab 2017b using previously reported methods.[22]

2.6. Analysis of Agronomic Traits. Factor analyses are a classical dimensionality reduction method that can effectively reduce the dimensionality of variables while retaining a large amount of valid information.[23] In this study, factor analysis was conducted using SPSS 26.0 for the synthesis of data on the nine agronomic traits of *A. tsao-ko*. Before factor analysis, the data were subjected to Kaiser−Meyer Olkin (KMO) test and Bartlett spherical test, KOM test mainly obtains the information on correlation strength between the variables, when the value of KMO is greater than 0.7 (the interval is 0−1), it indicates that the correlation strength is large, and the results of the factor analysis are reliable; Bartlett spherical test is mainly used to test the degree of correlation between the variables. Then, the factors were extracted using the principal component method and also rotated using the maximum variance rotation method, and the common factors were extracted based on the criterion that the lowest variance contribution was greater than 60%, which were used to represent the information on nine agronomic traits of *A. tsao-ko* at four maturity stages.

2.7. Spectral Data Analysis. In the process of collecting spectral data, it is easy to be affected by external factors and sample specifications, which will produce bad conditions such as baseline drift, noise pollution, light scattering effect, etc., which is not conducive to the analysis of spectral features and the establishment of models.[24] Therefore, before building a classification model, the raw spectral data are often preprocessed appropriately to improve the classification correctness and stability of the model. In this study, both FT-NIR and FT-MIR spectral data were subjected to five common preprocesses, including Baseline (BL), second derivative (second), multiplicative scatter correction (MSC), Savitzy-Golay (SG), and exponentially weighted moving average (EWMA). Then, based on the original spectral data

https://doi.org/10.1021/acsomega.4c03717
ACS Omega 2024, 9, 29857−29869

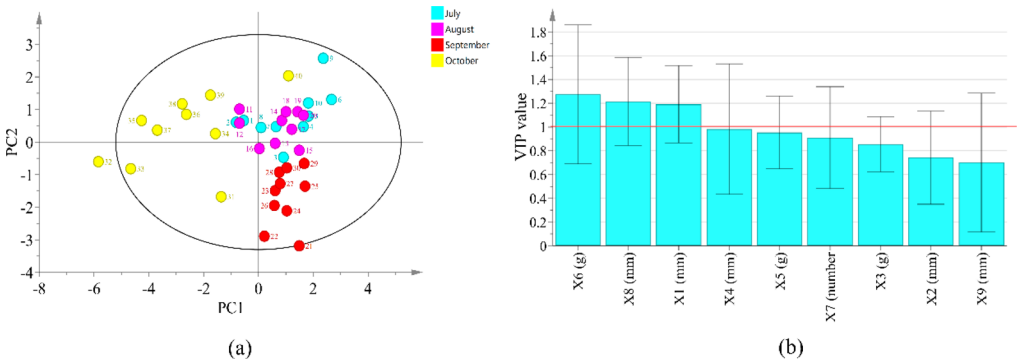

Figure 1. Agronomic traits of *A. tsao-ko* in four harvesting months were analyzed by partial least-squares discriminant analysis (PLS-DA): (a) Score plot and (b) variable importance in the projection (VIP).

and the preprocessed spectral data, the individual spectral data sets were divided into about 60% training set and 40% test set using the Kennard−Stone (KS) algorithm for building the PLS-DA model. In this work, the R^2 and Q^2 parameters are used to evaluate the stability of the model and its ability to predict new data, with the closer the value of both to 1, the better the performance of the model. In addition, the stability of the model is evaluated by the root-mean-square error of cross-validation (RMSECV) and the root-mean-square error of prediction (RMSEP). The closer the error value is to 0, the more stable the model is. To check the fit of the model, this study further conducted permutation tests for 200 iterations.

In addition, for the obtained 2DCOS images, after characterization, image recognition was further performed by ResNet for the identification of *A. tsao-ko* during different harvesting months. Before modeling, all the 2DCOS images are preprocessed and all the images are normalized to a size of 128 × 128 pixel, so the images are stored in JPEG format.

This study follows the previous research methodology to further validate the generalization ability of 2DCOS images combined with ResNet models in the identification of different harvesting months.[13] 70% of the 2DCOS images are used as a training set to build the model, and 30% of the images are used as a test set to test the stability and accuracy of the model. Based on the identity block and conv block, a ResNet model with a learning rate of 0.01 and a weight decay coefficient λ of 0.0001 was developed and applied to identify *A. tsao-ko* in different harvesting periods.

2.8. Metabolite Identification and Data Analysis. The annotations from the NIST2014 database were used to obtain the names of possible metabolites in each sample and their retention times, CAS numbers, relevant contents, etc. This annotated information for each sample was integrated to obtain the final metabolites used for analysis. In order to be able to compare data of different magnitudes, all peak areas were normalized to the internal standard using 1, 2-dichlorobenzene (100 μg/mL × 10 μL) (internal standard substance).

SIMCAP 14.0 (Umetrics AB, Umea, Sweden) was used to perform principal component analysis and partial least-squares discriminant analysis on the GC-MS data to further obtain information on the variability between the different categories of samples. Subsequently, metabolites with variable projection importance analysis values (VIP) > 1 (P < 0.05) were determined to be differential metabolites across the four harvest months based on Student t-test.

2.9. Network Pharmacology Analysis. *2.9.1. Collection of Potential Targets for Components and Diseases.* In this work, 80 potential targets of compounds were obtained by using databases such as TCMSP (http://lsp.nwu.edu.cn/tcmsp.php),[25] STITCH (https://stitch.embl.de/),[26] PubChem (https://pubchem.ncbi.nlm.nih.gov),[27] UniProt (https://www.uniprot.org/),[28] Use GeneCards (https://www.genecards.org/), OMIM (https://www.omim.org/), and TTD (https://db.idrblab.net/ttd/)[29] databases to collect obesity-related targets.

2.9.2. Construction of a Protein−Protein Interaction (PPI) Network. Based on 2.9.1, the targets of the compounds in *A. tsao-ko* were selected as intersecting targets with obesity-related targets, and they were imported into the STRING database (https://string-db.org/) for the initial construction of the PPI network. In this work, the organism was set as "Homo sapiens" and the data were exported to Excel and TSV formats.[30] Subsequently, the exported data were imported into Cytoscape 3.7.2 for visual analysis and data mining, and targets with a degree value greater than or equal to two times the median value were identified as core targets, which were used to map the active ingredient-core target network and analyze the potential mechanism of *A. tsao-ko* for the treatment of obesity.

2.9.3. KEGG Pathway Enrichment Analysis. To further investigate the key signaling pathways of *A. tsao-ko* for the treatment of obesity, KEGG signaling pathway analysis was performed using the Metascape database (Metascape, http://metascape.org/).[31] The core targets screened in 2.9.3 were imported into the DAVID database, and OFFICIAL_GENE_SYMBOL was selected as the identifier, the organism was set as "Homo sapiens" to obtain the KEGG-enriched signaling pathways, and those with P < 0.05 were identified as the key pathways.

3. RESULTS

3.1. Analysis of Agronomic Traits. *3.1.1. Variable Importance in the Projection Analysis.* In order to study the changes in morphological characteristics during the ripening process of *A. tsao-ko*, a supervised PLS-DA model was established for analysis using the agronomic traits of *A. tsao-ko* fruit as variables and 40 samples from July, August, September, and October as research subjects. The results of the model are shown in Figure 1, and the cumulative data explanatory parameters R^2X and R^2Y were 0.81 and 0.612, respectively, which were both greater than 0.5, indicating that the model has good stability, strong predictive ability, and can be used to distinguish between different maturity stages of *A.*

https://doi.org/10.1021/acsomega.4c03717
ACS Omega 2024, 9, 29857−29869

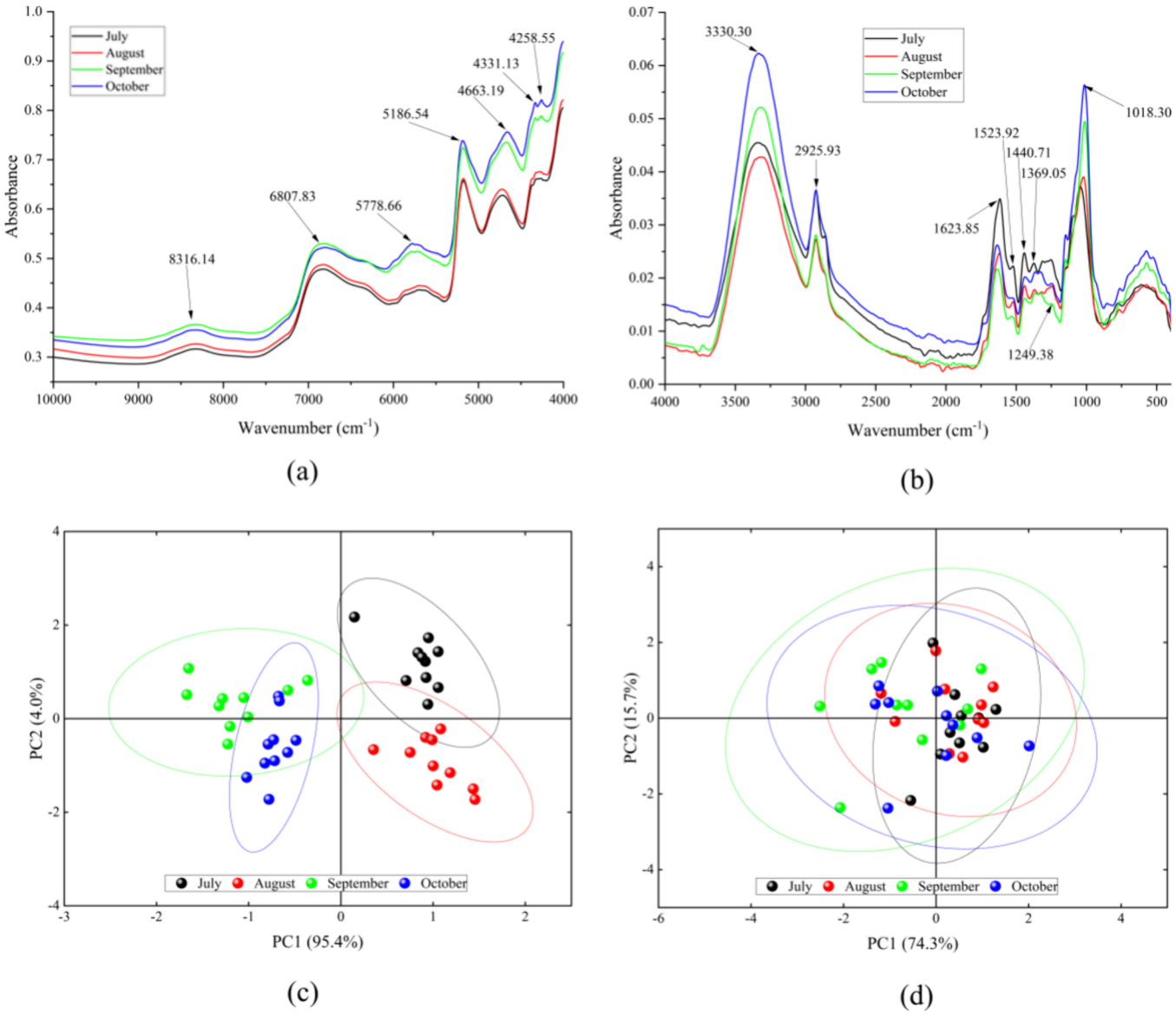

Figure 2. Plots of (a) FT-NIR and (b) FT-MIR averaged spectra of *A. tsao-ko* at different maturity stages. (c) Plot of PCA scores based on FT-NIR spectra. (d) Plot of PCA scores based on FT-MIR spectra.

tsao-ko. The score plot of the PLS-DA model is shown in Figure 1a, indicating significant morphological differences between *A. tsao-ko* at different maturity stages. Of these, the September samples were mainly concentrated in quadrant IV, the October samples were mainly concentrated in quadrants II and III, and the July and August samples overlapped and were distributed in quadrant I. This result indicated that there was greater variability in the agronomic traits between the samples from September and October and the samples from the other ripening periods. The overlap of the July and August samples may be due to the fact that these two months are in the early stages of maturation of *A. tsao-ko* and have less phenological variability.

To obtain the most variable agronomic traits during maturation of *A. tsao-ko*, we further calculated nine agronomic traits VIP scores were further calculated. VIP is mainly used to explain the contribution of the variables to the model, and VIP > 1 is usually used as a selection indicator.[32] Based on this, the results of ranking the nine agronomic traits are shown in Figure 1b. length of fruit, weight of seeds, and transverse diameter of seed all have VIP values greater than 1, which are the variables that contribute more to the classification performance of the model and also may be the ones that are more variable in the maturation process of *A. tsao-ko* Agronomic traits.

3.1.2. Factor Analyses. Factor analysis, as a classical comprehensive analysis method, is an important tool for assessing the quality and authenticity of agricultural products, and is commonly used in the comprehensive analysis of characteristic agronomic traits of agricultural products.[23] In this project, nine agronomic traits were factor analyzed in 40 samples of *A. tsao-ko* at four maturity stages. The results of KMO and Bartlett spherical test are shown in Table S2, and the value of KMO is 0.755, which is already greater than 0.6, indicating that there is a good correlation between the variables; The *p*-value of 0.000 for the Bartlett spherical test has been less than 0.05, indicating that the assumption of independence of the variables meets the criteria and the data set can be used to construct a factor analysis model. As shown in Table S3, the cumulative contribution of the first four

https://doi.org/10.1021/acsomega.4c03717
ACS Omega 2024, 9, 29857−29869

principal factors was 84.613%, indicating that these principal component factors were able to represent the information on agronomic traits of *A. tsao-ko* at different maturity stages and could be used for the comprehensive evaluation of *A. tsao-ko*.

In order to clarify the loading capacity of the factors, the maximum variance method was further applied to the common factor was rotated, and the rotated factor loading values are shown in Table S4. The first principal factor was mainly determined by width of fruit, weight of fruit, weight of peel, weight of seeds and number of seeds with a contribution of 38.208% and an eigenvalue of 3.439. The second principal factor was mainly determined by length of fruit and longitudinal diameter of seeds with a contribution of 18.974% and an eigenvalue of 1.708. The third principal factor was mainly determined by transverse diameter of seed with a contribution of 13.805% and an eigenvalue of 1.242. The fourth principal factor is mainly determined by thickness of peel with a contribution of 13.627% and an eigenvalue of 1.226.

Based on the four principal factors, a data model for the comprehensive evaluation of *A. tsao-ko* at different maturity stages was developed. The factor scores and composite factor scores of the model were calculated, and the results are shown in Table S5. The results were ranked according to the composite factor scores, and the average composite factor scores were calculated for different maturity stages, with *A. tsao-ko* collected in October having a high composite factor score. This result shows that *A. tsao-ko* in October is qualitatively superior from the point of view of *A. tsao-ko*'s morphological characteristics. However, evaluating the quality of *A. tsao-ko* from the combined score of the morphological characters alone is not comprehensive enough. Therefore, in the present study, FT-NIR and FT-MIR spectroscopic techniques were further employed for comprehensive chemical information characterization and differential chemical information analysis of *A. tsao-ko* at different maturity stages.

3.2. Spectral Analysis. Spectroscopy is an important tool that enables rapid analysis of the overall chemical information on a sample and has been widely used for chemical characterization and differential analysis of medicinal plants and edible mushrooms.[33,34] In this study, FT-NIR (10000−4000 cm^{-1}) and FT-MIR (4000−400 cm^{-1}) spectral data of all samples were collected separately to characterize the chemical information on *A. tsao-ko* at different maturity stages. The FT-NIR spectra of *A. tsao-ko* at different maturity stages are shown in Figure 2a, where seven common characteristic absorption peaks can be observed with some differences in the absorbance intensity. The characteristic peak near 8316.14 cm^{-1} is caused by the second overtone of the C−H stretch and may be related to the aliphatic compounds in *A. tsao-ko*.[35] The characteristic peaks near 6807.83 and 5778.66 cm^{-1} are mainly caused by O−H, N−H modes, and C−H stretched overtones which may be associated with polyphenols, polysaccharides and cellulose.[36] The characteristic peak near 5186.54 cm^{-1} is attributed to the first overtone of O−H stretching and C−O distortion, which is mainly present in water and polysaccharides.[37] The characteristic peak near 4663.19 cm^{-1} corresponds to a combination of C−O stretching and O−H deformation, which may be related to polysaccharides and polyphenols. The absorption band around 4331.13 cm^{-1} to 4258.55 cm^{-1} is mainly associated with a combination of C−C and C−H stretching absorption, probably related to glucose and cellulose.[38]

The FT-MIR spectra of *A. tsao-ko* at different maturity stages are shown in Figure 2b, and the broadband peak near 3330.30 cm^{-1} corresponds to the telescopic vibration of the O−H group, which may be associated with water, alcohols, phenols and other aromatic compounds.[18] There is a strong absorption peak near 2952.93 cm^{-1}, which is mainly caused by the asymmetric stretching vibration of $-CH_2$. The absorption peak near 1623.85 cm^{-1} can be attributed to the stretching vibrations of amide I and C═O, associated with the abundance of flavonoids in *A. tsao-ko*.[15] The absorption bands around 1523.92 cm^{-1}, 1440.71 cm^{-1}, and 1369.05 cm^{-1} are mainly caused by C−H bond stretching and bending vibrations in the $-CH_3$ and $-CH_2$ groups.[39] The region of 1350−400 cm^{-1} serves as the fingerprint region of the FT-MIR spectra, which is mainly due to the stretching vibrations of the single bonds such as C−C, C−N, and C−O and the skewed vibrations of the groups such as $-CH_3$, $-CH_2$, and $-NH_2$ in aliphatic compounds, saponins, polysaccharides, proteins, and polyphenolic compounds.[40]

Overall, FT-NIR spectroscopy in the region of 10000−4000 cm^{-1} was able to achieve differential characterization of the chemical information on *A. tsao-ko* at different maturity stages. Especially near the seven shared characteristic peaks, the absorbance values of all samples showed a pattern of October > September > August > July. Therefore, FT-NIR spectra have the potential to be used as fingerprints to distinguish between different maturation stages of *A. tsao-ko*. From the FT-MIR spectra, it can be observed that in the region of 1750−400 cm^{-1}, the spectra of *A. tsao-ko* of different maturity stages showed significant differences in peak shapes, peak positions and absorbance intensities, and only in the region of 1350−400 cm^{-1} the absorbance intensities of *A. tsao-ko* of different maturity stages showed a pattern of October > September > August > July. Of these, the regularity of the characteristic peak near 1018.30 cm^{-1} was significant. Therefore, the region 1350−400 cm^{-1} in the FT-MIR spectra can be used as a fingerprint region to distinguish between different maturity stages of *A. tsao-ko*.

3.3. Principal Component Analysis. PCA was a classical clustering method that reduces the dimensionality of the data while retaining a large amount of information in the data set, and ultimately demonstrates the mathematical distribution of the samples in space in the form of a score plot, which can visually assess the similarities and differences between the samples.[41] Based on the spectral analysis, further principal component analysis was performed for the variability analysis of the overall chemical information on *A. tsao-ko* at different maturity stages.

Figure 2c shows a plot of the PCA scores based on the FT-NIR spectral data, with PC1 (95.4%) and PC2 (4.0%) explaining 99.4% of the total variance, indicating that the first two principal components were able to characterize all of the spectral variables. In addition, it can be observed from the score plot that all of the samples were divided into four groups, indicating a more pronounced variability among *A. tsao-ko* at different stages of maturity. Interestingly, there is an overlap in the PCA score graphs for the July and August samples as well as for the September and October samples, which may be due to the fact that the chemical information is more similar because July and August serve as the early stages of *A. tsao-ko* maturation. The September *A. tsao-ko* is close to maturity, so it has chemical information similar to that of the October *A. tsao-ko*. Overall, the chemical variability between *A. tsao-ko* at

https://doi.org/10.1021/acsomega.4c03717
ACS Omega 2024, 9, 29857−29869

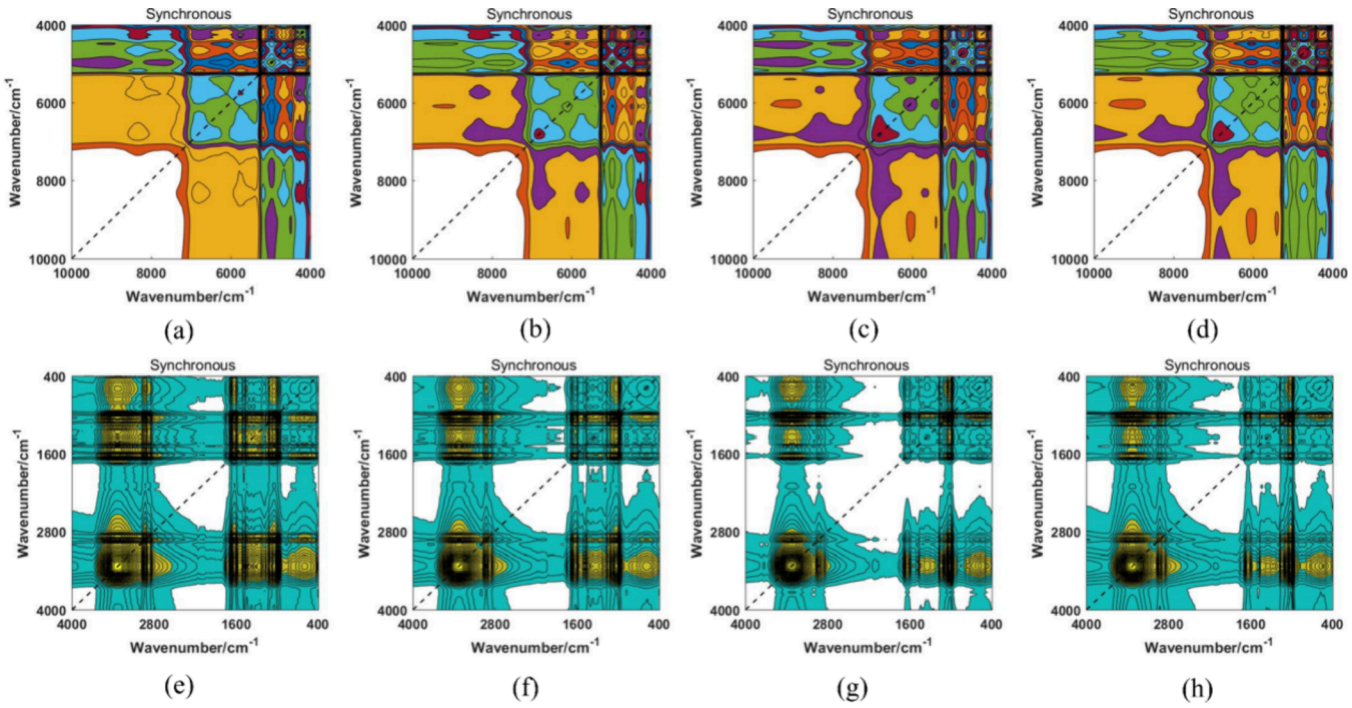

Figure 3. Synchronous 2DCOS images based on FT-NIR spectra of (a) *A. tsao-ko* in July, (b) *A. tsao-ko* in August, (c) *A. tsao-ko* in September, and (d) *A. tsao-ko* in October. Synchronous 2DCOS images based on FT-MIR spectra of (e) *A. tsao-ko* in July, (f) *A. tsao-ko* in August, (g) *A. tsao-ko* in September, and (h) *A. tsao-ko* in October.

different stages of maturity is more pronounced, in agreement with the results of the spectral analysis in section 3.2. Figure 2d shows a plot of the PCA scores based on the FT-MIR spectral data, with the first two principal components explaining 90.0% of the total variance, indicating that the first two PCs explain the overall chemical information on the sample. However, the *A. tsao-ko* samples from the four maturity stages overlapped more severely in the PCA score plots, and the separation was not significant. In summary, principal component analysis can estimate the distribution of a sample based on its FT-NIR spectral data and FT-MIR spectral data. However, FT-NIR can provide better discrimination of samples compared to FT-MIR.

3.4. Two-Dimensional Correlation Analysis. Generalized two-dimensional correlation spectra help to resolve possible correlations between different spectral features and can also be used to obtain the order of individual spectral variations.[42] Previous studies have shown that synchronous 2DCOS images are more suitable for analysis and identification for differential studies of medicinal plants with complex chemical component systems.[43,44] Therefore, synchronous 2DCOS images were acquired in this study for the characterization of chemical information and differential analysis of *A. tsao-ko* at different maturation stages in order to obtain the pattern of change in the chemical composition during the maturation of *A. tsao-ko*. Figure 3 shows synchronous 2DCOS images based on FT-NIR (a–d) and FT-MIR (e–h) spectra. From the images, it can be observed that both auto peaks (peaks located on the diagonal) and cross peaks (peaks located on both sides of the diagonal with symmetric properties) are present in the synchronous 2DCOS image. The intensity of auto peaks represents the sensitivity of the signal when the spectrum is subjected to external perturbation. Cross peaks reflect the existence of intermolecular or intramolecular interactions between functional groups, and positive cross peaks indicate that the functional groups respond in unison to external perturbations, and may be derived from the same or the same class of chemical constituents.[45]

Based on the synchronous 2DCOS images of FT-NIR spectra (Figure 3a–d), it can be observed that the auto peaks and cross peaks are mainly concentrated in the region of 7000–4000 cm^{-1}. One of the stronger auto peaks appeared near 6807.83 cm^{-1}, and the area of the peak gradually increased as *A. tsao-ko* matured. In addition, a similar trend was observed in the 5100–4000 cm^{-1} region, and the changes in auto peaks were mainly influenced by external disturbance signals, so the phenomenon may be related to the changes in the content of polysaccharides, polyphenols, and aliphatic compounds during the maturation process of *A. tsao-ko*. The number and complexity of cross peaks also increased with the maturity of *A. tsao-ko*, mainly due to the increase in the degree of inter- and intramolecular interactions, indicating that the number and content of chemical components increased during the maturation of *A. tsao-ko*. The synchronous 2DCOS images based on FT-MIR spectra (Figure 3e, h), which can observe the overall variability among *A. tsao-ko* at different maturity stages, were able to identify *A. tsao-ko* at different maturity stages. Unfortunately, it is difficult to observe the changing pattern of chemical composition during the maturation process of *A. tsao-ko* in synchronous 2DCOS images, which is consistent with the analytical results of 3.2, probably due to the strong sensitivity of FT-MIR spectroscopy.[46]

In summary, synchronous 2DCOS images based on FT-NIR spectroscopy were able to better characterize the overall chemical change pattern during the maturation process of *A. tsao-ko* and changes in the content of polysaccharides, polyphenols, and aliphatic compounds could be observed. Unfortunately, synchronous 2DCOS images can only obtain differential variations in the overall chemical information,

https://doi.org/10.1021/acsomega.4c03717
ACS Omega 2024, 9, 29857–29869

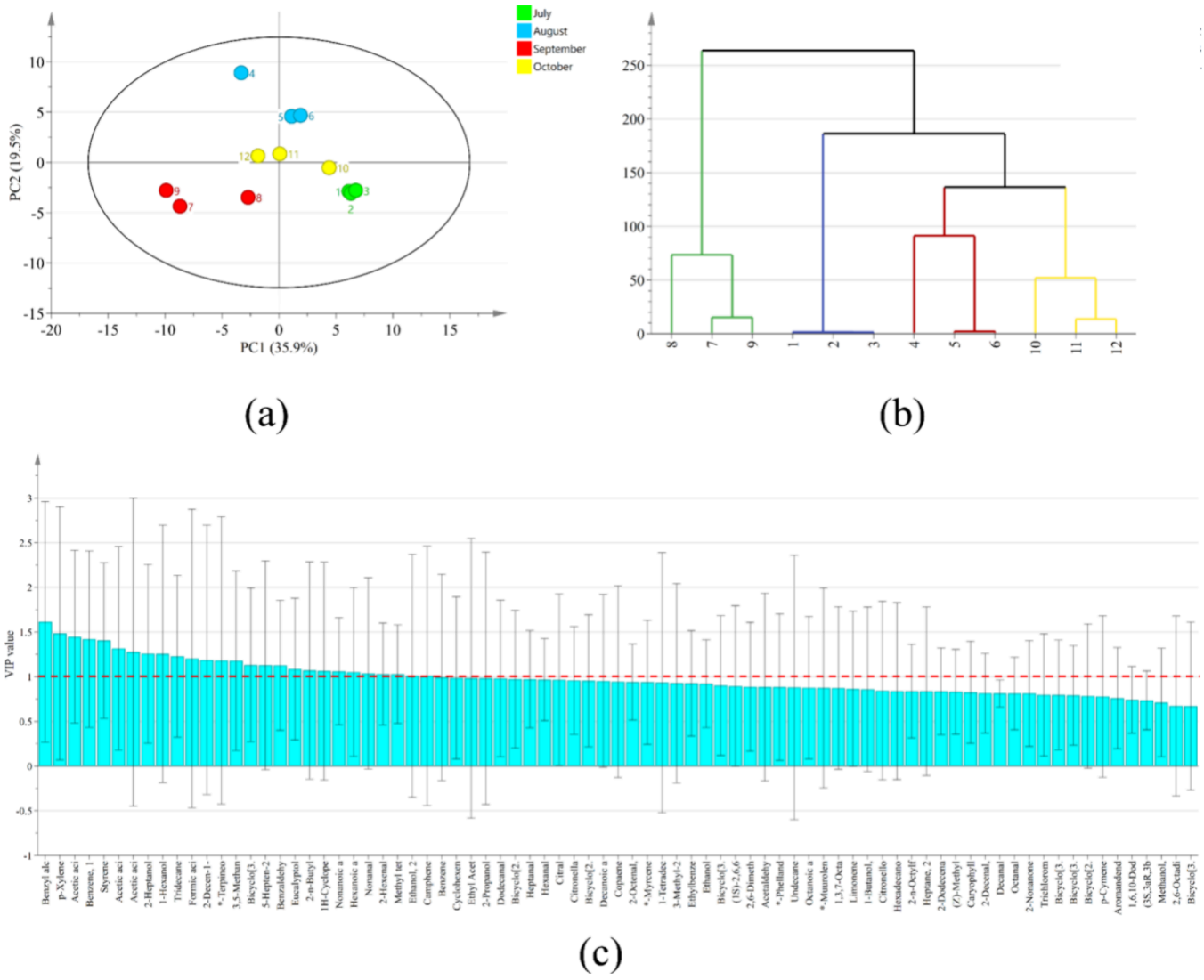

Figure 4. PLS-DA and HCA based on GC-MS data: (a) Plot of PLS-DA scores, (b) HCA dendrogram, and (c) VIP scores.

making it difficult to obtain detailed information on the chemical composition and its content. Therefore, GC-MS analysis was carried out on the basis of the overall analysis by spectroscopic techniques to further analyze the detailed patterns of changes in the chemical composition and content during the maturation process of *A. tsao-ko*.

3.5. GC-MS Analysis. Based on GC-MS technology, 80 compounds were identified from *A. tsao-ko* in July, August, September, and October, mainly including aliphatic, aromatic, and terpenoids. Detailed chemical information is shown in Table S6, with 54 detected in samples collected in July, 63 detected in *A. tsao-ko* collected in August, and 68 detected in both samples collected in September and October, respectively.

In order to investigate the main cause of the variability shown in the FT-NIR and FT-MIR spectra, the GC-MS data were further analyzed using chemometrics for differential metabolites in *A. tsao-ko* at different maturity stages. PLS-DA is a classical supervised classification method with the ability of data dimensionality reduction, data mining, and data categorization, which has been widely used in classification identification, content prediction, and metabolomics analysis.[47,48] In this work, a PLS-DA model was developed for the GC-MS data set after normalizing the peak area of internal markers with 80 components as variables and different maturity stages as classification labels. The results of PLS-DA are shown in Figure 4, where the number of optimal LVs is 6, R^2X is 0.891, R^2Y is 0.988, and Q^2 is 0.874, indicating the superiority of the model's in explaining the data and predicting the performance. The PLS-DA apparent score plot is shown in Figure 4a, with a more significant trend of sample separation across the 4 maturation stages, with PC1 and PC2 together explaining 55.4% of the total variance. The HCA dendrogram is shown in Figure 4b, where all samples were categorized into 4 classes when the distance was less than 100, indicating a high variability in chemical composition and content between samples of different maturity stages. The VIP index quantifies the contribution of each variable to the categorization.[49] In general, when a variable has a VIP score greater than 1, it can be defined as a key variable in the categorization process. As shown in Figure 4c, this work screened a total of 20 key variables as differential metabolites of *A. tsao-ko* at different maturity stages (July, August, September, and October) based on the PLS-DA model with VIP > 1, $p < 0.05$ as the screening criterion, including benzyl alcohol (NO. 60), *p*-xylene (NO. 2), Acetic acid (NO. 4), styrene (NO. 67), acetic acid, methyl

https://doi.org/10.1021/acsomega.4c03717
ACS Omega 2024, 9, 29857−29869

Table 2. Identification of Differential Metabolites in the Chemical Components of *A. tsao-ko* Coming July, August, September, and October

Name	CAS	rt	VIP	p. value	FDR
Benzyl alcohol (alcohol)	100-51-6	32.1524	1.61371	0.000250569	0.006715
p-Xylene (aromatic)	106-42-3	8.624117	1.48537	0.000153908	0.005236
Acetic acid (acids)	64-19-7	18.20706	1.44759	0.000156308	0.005236
Styrene (aromatic)	100-42-5	12.54979	1.40543	5.07×10^{-05}	0.003397
Acetic acid, methyl ester (esters)	79-20-9	2.334951	1.31831	0.00545038	0.045647
Acetic acid, octyl ester (esters)	112-14-1	18.7667	1.27572	0.004557825	0.041267
2-Heptanol (alcohol)	543-49-7	14.53399	1.25682	0.07662019	0.220504
1-Hexanol (esters)	111-27-3	15.44281	1.25562	0.007785583	0.057959
Tridecane (hydrocarbons)	629-50-5	13.95249	1.22851	0.00113936	0.016125
Formic acid, octyl ester (esters)	112-32-3	20.9566	1.20354	0.019931575	0.110185
Ethanol, 2-butoxy- (ethers)	111-76-2	1.01082	1.193193	0.018211375	0.108655
2-Decen-1-ol, (*E*)- (alcohol)	18409-18-2	29.998	1.1887	0.078666012	0.220504
Bicyclo[3.1.1]hept-2-ene-2-methanol, 6,6-dimethyl- (alcohol)	515-00-4	28.77413	1.13188	0.000823799	0.01577
5-Hepten-2-one, 6-methyl- (ketone)	110-93-0	14.99235	1.12894	0.001796893	0.021889
2-*n*-Butyl furan (heterocyclic)	4466-24-4	8.684472	1.06914	0.015716489	0.100286
Nonanoic acid, methyl ester (esters)	1731-84-6	19.17992	1.06082	0.029645767	0.132418
Hexanoic acid, methyl ester (esters)	106-70-7	10.45388	1.05189	0.005981768	0.04715
Nonanal (aldehydes)	124-19-6	16.56962	1.03724	0.049179013	0.173717
2-Hexenal (aldehydes)	505-57-7	11.40417	1.02989	0.033202893	0.143522
Methyl tetradecanoate (esters)	124-10-7	37.36423	1.02891	0.001203339	0.016125

ester (NO. 10), acetic acid, octyl ester (NO. 73), 2-heptanol (NO. 35), 1-hexanol (NO. 72), tridecane (NO. 34), formic acid, octyl ester (NO. 48), ethanol, 2-butoxy- (NO. 68), 2-decen-1-ol, (E)- (NO. 59), bicyclo[3.1.1]hept-2-ene-2-methanol, 6,6-dimethyl- (NO. 56), 5-hepten-2-one, 6-methyl- (NO. 36), 2-*n*-butyl furan (NO. 22), nonanoic acid, methyl ester (NO. 44), hexanoic acid, methyl ester (NO. 28), nonanal (NO. 39), 2-hexenal (NO. 71), methyl tetradecanoate (NO. 62). The information on all the differential metabolites is shown in Table 2, which is mainly composed of alcohol, aromatic, acids, esters, hydrocarbons, ketone, heterocyclic, and aldehydes, indicating that these components are important factors for the chemical differences between *A. tsao-ko* at different maturity stages. From the point of view of chemical bonding and functional groups, these compositions mainly contain C−H, N−H, O−H, $-CH_3$, $-CH_2$, C═O, and $-NH_2$, etc. This result can better explain the differences of the characteristic peaks present in the FT-NIR and FT-MIR spectra.

3.6. Network Pharmacology Analysis. In order to further gain the potential of *A. tsao-ko* in the prevention, treatment or adjuvant treatment of obesity, a "component-target-disease-pathway" network model was established based on 80 components detected in 3.5, and the antiobesity activity of *A. tsao-ko* was preliminarily studied. As shown in Figure 5a, 581 targets related to components and 9873 targets related to obesity were collected from databases such as Swiss Target Predicate, GeneCards, UniProt, and DisGeNET. According to the Venn diagram results, there are 408 common targets between component targets and obesity targets (Figure 5a). Figure 5b and c shows the PPI network maps for intersecting targets (408) and core targets (85), respectively. The size of the node indicates the degree value; the larger the node, the higher the degree value, the thicker the edge line, the higher the median value, and the corresponding target is likely to be a core target.[50] In this work, values greater than two times the median of the target's degree value were used as a screening criterion to obtain core targets, and details of the 85 core

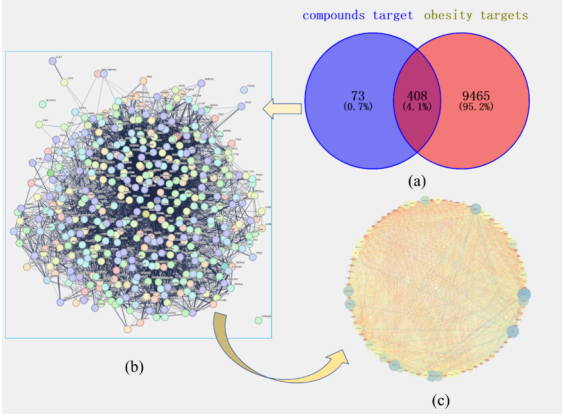

Figure 5. (a) Intersecting targets of component targets and disease targets, (b) PPI network of all targets, and (c) PPI network of core targets.

targets are shown in Table S7. In KEGG pathway enrichment analysis, a total of 162 signaling pathways were obtained ($p < 0.05$). Figure 6 shows the results of KEGG enrichment analysis based on the core targets, with bubble plots showing the top 20 signaling pathways ($p < 0.05$), including PI3K-Akt signaling pathway, Endocrine resistance, Chemical carcinogenesis - receptor activation, AGE-RAGE signaling pathway in diabetic complications, Lipid and atherosclerosis. The results suggest that the chemical constituents in *A. tsao-ko* are mainly distributed in multiple metabolic pathways, which have coordinated interactions with each other and treat or assist in the treatment of obesity by modulating adipocyte differentiation effects and inhibiting fat accumulation.[4,5]

In order to investigate the potential mechanism of action of *A. tsao-ko* for the treatment of obesity, a network pharmacology model was further developed based on the above screening and analysis. The structure of the network is shown in Figure 7, which consists of 27 compounds, 85 key targets, 20 important signaling pathways, and 1 disease

https://doi.org/10.1021/acsomega.4c03717
ACS Omega 2024, 9, 29857−29869

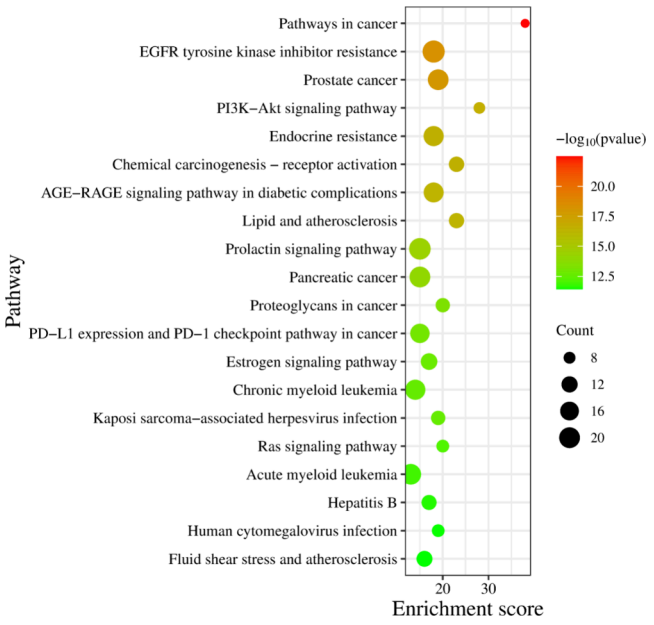

Figure 6. KEGG enrichment pathways of core targets (top 20).

(obesity), forming a "component−target−disease−pathway" network with 132 nodes and 508 edges. From the network, it can be observed that each component corresponds to more targets, and the targets are connected with different signal pathways, indicating that *A. tsao-ko* has the characteristics of "multi-component, multi-target, and multi-pathway" in the treatment or adjuvant treatment of obesity, and there is synergy between different treatment pathways.[27,51] Among them, decanoic acid, metal ester (NO. 50), nonanoic acid, methyl ester (NO. 44), dodecanal (NO. 54), (Z) -methyl hexadec-11-enoate (NO. 64), decanal (NO. 45), 1,6,10-dodecatrien-3-ol, 3,7,11-trimethyl- (NO. 8), 2-nonanone (NO. 37) have higher degree values, indicating that these components may be potential active ingredients for the treatment or adjuvant treatment of obesity.

4. DISCUSSION

The objective of the present study was mainly to characterize the changes in chemical composition, chemical information variability, quality, and medicinal potential of *A. tsao-ko* at different stages of maturity. In order to achieve this goal, the present study was based on multiple perspectives of agronomic traits morphological traits changes, phytochemistry, and phytopharmacology and used a combination of various analytical techniques, such as FT-NIR spectroscopy, FT-MIR spectroscopy, GC-MS, chemometrics, factorial analysis, two-dimensional correlation analysis, and differential metabolite analysis for the comprehensive *A. tsao-ko* at different maturity stages analysis and chemical information characterization. In addition, a network pharmacological analysis was used in this study to search for potential targets of A. tsao-ko chemical constituents and to explore their potential value in the treatment or adjunctive treatment of obesity.

From the point of view of morphological characteristics, the variability of *A. tsao-ko* at different maturity stages was mainly in the seeds. As shown in Figure S1, there was not much variability in fruit shape as the fruit matured, but the color of the internal seeds gradually changed from white to brown. Based on this finding, in the present study, ten fruits were randomly selected from *A. tsao-ko* samples of each month and nine agronomic traits such as length of fruit, width of fruit, transverse diameter of seed were further determined and factor analyzed, which showed that *A. tsao-ko* in October had a morphology had a relative advantage. And these agronomic traits are mainly associated with the yield of *A. tsao-ko*, so October may be the potential yielding period.[23]

From the chemical components point of view, the FT-NIR spectra in the region of 10,000−4,000 cm^{-1} all visualize the variability between different months, and the absorbance intensity shows a trend of October > September > August > July. The FT-MIR spectra showed the above trend only in the fingerprint region (1350−400 cm^{-1}), which may be due to the high sensitivity of the FT-NIR spectra, and therefore the greater degree of interference, and the complex chemical composition system of *A. tsao-ko*, so that it is difficult to differentiate in the other regions of the overlap is severe.[18] The results of GC-MS analysis indicated that the O−H, C−H, N−H, and C═O bonds in alcohol, aromatic, acids, esters, hydrocarbons, ketone, heterocyclic, and aldehydes may be important in causing the characteristic peaks in the spectra.

From a pharmacological point of view, decanoic acid, methyl ester (NO. 50), nonanoic acid, and methyl ester (NO. 44), dodecanal (NO.54), (*Z*)-methyl hexadec-11-enoate (NO. 64),

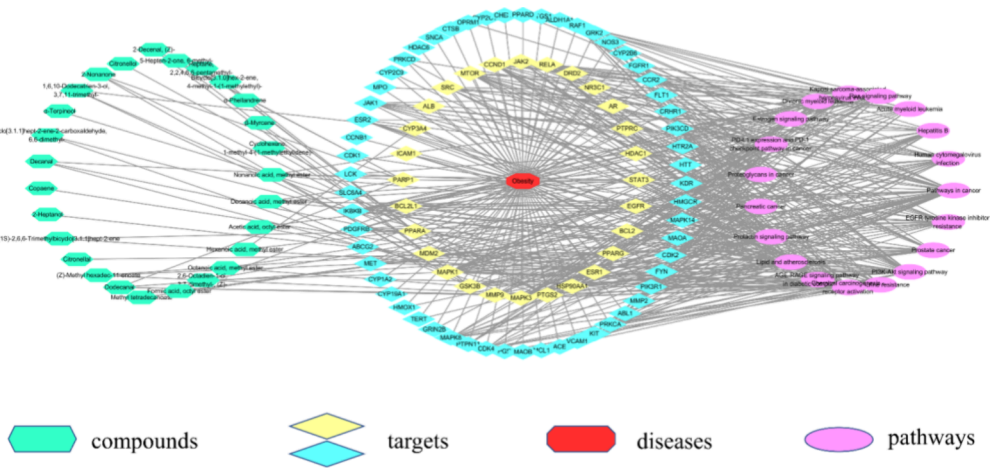

Figure 7. "component-target-disease-pathway" network.

https://doi.org/10.1021/acsomega.4c03717
ACS Omega 2024, 9, 29857−29869

decanal (NO. 45), 1,6,10-dodecatrien-3-ol, 3,7,11-trimethyl- (NO. 8), and 2-nonanone (NO. 37) may be potentially active ingredients. There is no direct indication in the published studies that *A. tsao-ko* therapeutic activity for obesity is related to these components, but it has been demonstrated that the ethanol extract of *A. tsao-ko* effectively inhibits the accumulation of visceral and subcutaneous fat,[52−54] so it can be hypothesized that these components may be the active ingredients in the treatment of obesity by *A. tsao-ko*. However, these components are mainly volatiles and need to be made into other types of agents during application in order to improve bioavailability.[55,56] These potential active components were somewhat different in *A. tsao-ko* at different maturity stages, and detailed results are shown in Table S6. In contrast, the relative content of these active ingredients was higher in *A. tsao-ko* in September and October, and October was the mature period with the highest accumulation of active ingredients, which could be the best time for raw material collection for the treatment of obesity.

In conclusion, among the different maturity periods, *A. tsao-ko* in October has superior agronomic traits, occupies a higher position in terms of chemical composition and content, and has a higher relative content of potential active ingredients, suggesting that *A. tsao-ko* in October is of relatively high quality and can be used as a potential harvesting period for *A. tsao-ko*. In addition, FT-NIR and FT-MIR spectra and the corresponding 2DCOS images can characterize the chemical information on *A. tsao-ko* at different maturity stages from a macroscopic point of view, which has a high potential for application as a fast, convenient, and accurate detection and analysis technique. Spectroscopy combined with GC-MS technology and network pharmacology was applied to analyze and characterize the chemical information on *A. tsao-ko* at different maturity stages, which provided a comprehensive analytical platform for the quality evaluation study of *A. tsao-ko*, and new ideas for the development of finishing products of *A. tsao-ko*. Unfortunately, this study only explored the potential of *A. tsao-ko* for the treatment of obesity based on the preliminary network pharmacology, and further corresponding validation experiments need to be carried out in subsequent studies to explore the main mechanism of *A. tsao-ko* for the treatment of obesity in depth.

5. CONCLUSIONS

In the present study, the agronomic traits of *A. tsao-ko* were analyzed and the results of factor analysis showed that the composite score of *A. tsao-ko* was relatively high in October, which provided a basis for the preliminary evaluation of the quality of *A. tsao-ko* at different maturity stages. In addition, for the first time, FT-NIR, FT-MIR, and GC-MS techniques were used to comprehensively analyze and visually characterize the changes in chemical information on *A. tsao-ko* at different maturity stages. The results of spectral analysis showed that there was a high chemical variability among *A. tsao-ko* at different maturity stages and the absorbance intensity showed a trend of October > September > August > July. By GC-MS analysis, 54, 63, 68, and 68 chemical components were detected from *A. tsao-ko* at different maturity stages, and 20 differential metabolites were screened in combination with PLS-DA (VIP > 1, $p < 0.05$). Network pharmacological analysis screened decanoic acid, methyl ester (NO. 50), nonanoic acid, methyl ester (NO. 44), dodecanal (NO. 54), (Z)-methyl hexadec-11-enoate (NO. 64), decanal (NO. 45), 1,6,10-dodecatrien-3-ol, 3,7,11-trimethyl- (NO. 8), 2-nonanone (NO. 37), and other potential chemical components, suggesting the potential of *A. tsao-ko* in the treatment or adjunctive treatment of obesity. All in all, the relatively high quality of *A. tsao-ko* in October may be an important ripening period for *A. tsao-ko* as well as a potential harvesting period. This study provides a comprehensive and integrated analytical platform for the harvesting and quality evaluation of *A. tsao-ko*, as well as a theoretical basis for the harvesting and product development of *A. tsao-ko*.

■ ASSOCIATED CONTENT

Supporting Information

The Supporting Information is available free of charge at https://pubs.acs.org/doi/10.1021/acsomega.4c03717.

A.tsao-ko phenotypes at different maturity stages: (a) *A.tsao-ko* in July; (b) *A.tsao-ko* in August; (c) *A.tsao-ko* in September; (d) *A.tsao-ko* in October; KMO and Bartlett's test results; Characteristic root of the correlation coefficient and the variance contribution rate; Factor loading matrix after rotation by factor analysis; Scores of each main factor, composite scores and ranking of *A. tsao-ko* at different stages of maturity; Compounds detected in *A. tsao-ko* at different maturity stages (PDF)

■ AUTHOR INFORMATION

Corresponding Authors

Shao-bing Yang − *Medicinal Plants Research Institute, Yunnan Academy of Agricultural Sciences, Kunming 650200, China*; Email: ysb9-116@163.com

Yuan-zhong Wang − *Medicinal Plants Research Institute, Yunnan Academy of Agricultural Sciences, Kunming 650200, China*; orcid.org/0000-0001-5376-757X; Email: boletus@126.com

Author

Gang He − *Medicinal Plants Research Institute, Yunnan Academy of Agricultural Sciences, Kunming 650200, China; College of Food Science and Technology, Yunnan Agricultural University, Kunming 650201, China*

Complete contact information is available at: https://pubs.acs.org/10.1021/acsomega.4c03717

Author Contributions

Gang He: Carried out the experiments, analyzed the data, wrote the original manuscript. Shao-bing Yang: Analyzed the data and participated in the discussion. Yuan-zhong Wang: Conceived the original idea for this study, supervised the whole project, reviewed, and edited the manuscript.

Notes

The authors declare no competing financial interest.

■ ACKNOWLEDGMENTS

I am grateful for the valuable comments from editors and reviewers. This work was supported by Yunnan Province Agricultural Basic Research Joint Special Project (Grant number: 202301BD070001-050), Special Program for the Major Science and Technology Projects of Yunnan Province (1. Grant number: 202202AE090001; 2. Grant number: 202102AE090051-1-01).

REFERENCES

(1) Fahey, J. W.; Kensler, T. W. Phytochemicals: Do they belong on our plate for sustaining healthspan? *Food Front.* **2021**, *2*, 235−239.
(2) Li, G. D.; Lu, Q. W.; Wang, J. J.; Hu, Q. Y.; Liu, P. H.; Yang, Y. W.; Li, Y. K.; Tang, H. R.; Xie, H. Correlation analysis of compounds in essential oil of *Amomum tsaoko* seed and fruit morphological characteristics, geographical conditions, locality of growth. *Agronomy* **2021**, *11*, 744.
(3) He, G.; Yang, S. B.; Wang, Y. Z. The potential of *Amomum tsao-ko* as a traditional Chinese medicine: Traditional clinical applications, phytochemistry and pharmacological properties. *Arab. J. Chem.* **2023**, *16*, 104936.
(4) Hong, S. S.; Choi, C. W.; Lee, J. E.; Jung, Y. W.; Lee, J. A.; Jeong, W.; Choi, Y.; Cha, H.; Ahn, E.; Oh, J. S. Bioassay-guided isolation and identification of anti-obesity phytochemicals from fruits of *Amomum tsao-ko*. *Appl. Biol. Chem.* **2021**, *64*, 2.
(5) Shim, K. S.; Hwang, Y. H.; Jang, S. A.; Kim, T.; Ha, H. Ethanol extract of *Amomum tsao-ko* ameliorates ovariectomy-induced trabecular loss and fat accumulation. *Molecules* **2021**, *26*, 784.
(6) Li, P.; Long, J. R.; Bai, G. X.; Zhang, J.; Cha, Y. S.; Gao, W. J.; Luan, X. B.; Wu, L. Z.; Mu, M. X.; Kennelly, E. J.; et al. Metabolomics and Transcriptomics Reveal that Diarylheptanoids Vary in *Amomum tsao-ko* Fruit Development. *J. Agric. Food Chem.* **2023**, *71*, 7020−7031.
(7) Akpertey, A.; Krah Adu-Gyamfi, P. K.; Dadzie, A. M. Genetic-base broadening of Robusta coffee: Assessment of genetic variability for vigor and yield of introduced germplasm. *Ecol. Genet.* **2022**, *25*, 100151.
(8) Alcântara, J. F. D.; Santos, R. G. D.; Baio, F. H. R.; Silva Júnior, C. A. D.; Teodoro, P. E.; Teodoro, L. P. R. High-throughput phenotyping as an auxiliary tool in the selection of corn hybrids for agronomic traits. *Rev. Ceres* **2023**, *70*, 106−113.
(9) Santana, D. C.; Dos Santos, R. G.; Teodoro, L. P. R.; Da Silva Junior, C. A.; Baio, F. H. R.; Coradi, P. C.; Teodoro, P. E. Structural equation modelling and factor analysis of the relationship between agronomic traits and vegetation indices in corn. *Euphytica.* **2022**, *218*, 44.
(10) He, G.; Lin, Q.; Yang, S. B.; Wang, Y. Z. A rapid identification based on FT-NIR spectroscopies and machine learning for drying temperatures of *Amomum tsao-ko*. *J. Food Compos. Anal.* **2023**, *118*, 105199.
(11) Zhang, J.; Wang, Y. Z.; Yang, M. Q.; Yang, W. Z.; Yang, S. B.; Zhang, J. Y. Identification and evaluation of *Polygonatum kingianum* with different growth ages based on data fusion strategy. *Microchem J.* **2021**, *160*, 105662.
(12) Zhang, Y. Y.; Wang, Y. Z. Machine learning applications for multi-source data of edible crops: A review of current trends and future prospects. *Food Chem. X* **2023**, *19*, 100860.
(13) He, G.; Yang, S. B.; Wang, Y. Z. An integrated chemical characterization based on FT-NIR, and GC-MS for the comparative metabolite profiling of 3 species of the genus *Amomum*. *Anal. Chim. Acta* **2023**, *1280*, 341869.
(14) Yan, Z. Y.; Liu, H. G.; Li, J. Q.; Wang, Y. Z. Qualitative and quantitative analysis of *Lanmaoa asiatica* in different storage years based on FT-NIR combined with chemometrics. *Microchem J.* **2023**, *189*, 108580.
(15) Yue, J. Q.; Li, Z. M.; Zuo, Z. T.; Zhao, Y. L.; Zhang, J.; Wang, Y. Z. Study on the identification and evaluation of growth years for *Paris polyphylla* var. yunnanensis using deep learning combined with 2DCOS. *Spectrochim. Acta. A* **2021**, *261*, 120033.
(16) Qiu, S.; Cai, Y.; Yao, H.; Lin, C.; Xie, Y.; Tang, S.; Zhang, A. Small molecule metabolites: discovery of biomarkers and therapeutic targets. *Signal Transduct. Target. Ther.* **2023**, *8*, 132.
(17) Wang, X. J.; Zhang, X. X.; Li, J. X.; Fu, J. Y.; Zhao, M. J.; Zhang, W. T.; Weng, W. L.; Li, Q. Y. Network pharmacology and LC-MS approachs to explore the active compounds and mechanisms of Yuanjiang decoction for treating bradyarrhythmia. *Comput. Biol. Med.* **2023**, *152*, 106435.
(18) Li, L.; Zhao, Y.; Li, Z.; Wang, Y. Multi-information based on ATR-FTIR and FT-NIR for identification and evaluation for different parts and harvest time of *Dendrobium officinale* with chemometrics. *Microchem J.* **2022**, *178*, 107430.
(19) Liu, C. L.; Shen, T.; Xu, F. R.; Wang, Y. Z. Main components determination and rapid geographical origins identification in *Gentiana rigescens* Franch. based on HPLC, 2DCOS images combined to ResNet. *Ind. Crop. Prod.* **2022**, *187*, 115430.
(20) Liu, Z. M.; Yang, S. B.; Wang, Y. Z.; Zhang, J. Y. Discrimination of the fruits of *Amomum tsao-ko* according to geographical origin by 2DCOS image with RGB and Resnet image analysis techniques. *Microchem J.* **2021**, *169*, 106545.
(21) Noda, I. Generalized Two-Dimensional correlation method applicable to Infrared, Raman, and other Types of Spectroscopy. *Appl. Spectrosc.* **1993**, *47*, 1329−1336.
(22) Dong, J. E.; Li, J. Q.; Liu, H. G.; Wang, Y. Z. Machine learning and deep learning based on the small FT-MIR dataset for fine-grained sampling site recognition of boletus tomentipes. *Food Res. Int.* **2023**, *167*, 112679.
(23) Liao, S. H.; Fan, Z. W.; Huang, X. J.; Ma, Y. R.; Huang, F. Y.; Guo, Y. A.; Chen, T. Q.; Wang, P.; Chen, Z. L.; Yang, M. S.; et al. Variations in the morphological and chemical composition of the rhizomes of *Polygonatum* species based on a common garden experiment. *Food Chem. X* **2023**, *17*, 100585.
(24) Rinnan, A.; Berg, F. v. d.; Engelsen, S. B. Review of the most common pre-processing techniques for near-infrared spectra. *Trac-Trend. Anal. Chem.* **2009**, *28*, 1201−1222.
(25) Li, X.; Wei, S. Z.; Niu, S. Q.; Ma, X.; Li, H. T.; Jing, M. Y.; Zhao, Y. L. Network pharmacology prediction and molecular docking-based strategy to explore the potential mechanism of Huanglian Jiedu Decoction against sepsis. *Comput. Biol. Med.* **2022**, *144*, 105389.
(26) He, S.; Wang, T. Q.; Shi, C. W.; Wang, Z. G.; Fu, X. J. Network pharmacology-based approach to understand the effect and mechanism of *Danshen* against anemia. *J. Ethnopharmacol.* **2022**, *282*, 114615.
(27) Zhou, W.; Zhang, H.; Wang, X.; Kang, J.; Guo, W. Y.; Zhou, L. H.; Liu, H. Y.; Wang, M. L.; Jia, R. K.; Du, X. J.; et al. Network pharmacology to unveil the mechanism of Moluodan in the treatment of chronic atrophic gastritis. *Phytomedicine* **2022**, *95*, 153837.
(28) Cui, X. Y.; Wu, X.; Lu, D.; Wang, D. Network pharmacology-based strategy for predicting therapy targets of Sanqi and Huangjing in diabetes mellitus. *World J. Clin. Cases* **2022**, *10*, 6900−6914.
(29) Li, L.; Zuo, Z. T.; Wang, Y. Z. Practical qualitative evaluation and screening of potential biomarkers for different parts of *Wolfiporia cocos* using machine learning and network pharmacology. *Front. Microbiol.* **2022**, *13*, 931967.
(30) Ge, Q.; Chen, L.; Tang, M.; Zhang, S.; Liu, L. L.; Gao, L.; Ma, S. S.; Kong, M.; Yao, Q.; Feng, F.; et al. Analysis of mulberry leaf components in the treatment of diabetes using network pharmacology. *Eur. J. Pharmacol.* **2018**, *833*, 50−62.
(31) Shi, S.; Luo, Y. F.; Ma, Y.; Chu, Y. J.; Wang, Y. D.; Chen, X. H.; Chu, Y. Identification of in vitro-in vivo components of Caoguo using accelerated solvent extraction combined with gas chromatography-mass spectrometry integrated with network pharmacology on indigestion. *Ann. Transl. Med.* **2021**, *9*, 1247.
(32) Du, H.; Chen, W. L.; Lei, Y. T.; Li, F. C.; Li, H. M.; Deng, W.; Jiang, G. H. Discrimination of authenticity of Fritillariae Cirrhosae Bulbus based on terahertz spectroscopy and chemometric analysis. *Microchem J.* **2021**, *168*, 106440.
(33) Liu, C. L.; Zuo, Z. T.; Xu, F. R.; Wang, Y. Z. Authentication of Herbal Medicines Based on Modern Analytical Technology Combined with Chemometrics Approach: A Review. *Crit. Rev. Anal. Chem.* **2023**, *53*, 1393−1418.
(34) Yan, Z. Y.; Liu, H. G.; Zhang, S.; Li, J. Q.; Wang, Y. Z. Superiority of two-dimensional correlation spectroscopy combined with ResNet in species identification of bolete. *Infrared Phys. Technol.* **2022**, *125*, 104303.
(35) He, G.; Yang, S. B.; Wang, Y. Z. The potential of *Amomum tsao-ko* as a traditional Chinese medicine: Traditional clinical applications,

https://doi.org/10.1021/acsomega.4c03717
ACS Omega 2024, 9, 29857−29869

phytochemistry and pharmacological properties. *Arab. J. Chem.* **2023**, *16*, 104936.
(36) Zhou, Y. P.; Jiang, J. H.; Wu, H. L.; Shen, G. L.; Yu, R. Q.; Ozaki, Y. Dry film method with ytterbium as the internal standard for near infrared spectroscopic plasma glucose assay coupled with boosting support vector regression. *J. Chemometr.* **2006**, *20*, 13−21.
(37) Liu, Z. M.; Yang, S. B.; Wang, Y. Z.; Zhang, J. Y. Multi-platform integration based on NIR and UV-Vis spectroscopies for the geographical traceability of the fruits of *Amomum tsao-ko*. *Spectrochim. Acta. A* **2021**, *258*, 119872.
(38) Amirvaresi, A.; Nikounezhad, N.; Amirahmadi, M.; Daraei, B.; Parastar, H. Comparison of near-infrared (NIR) and mid-infrared (MIR) spectroscopy based on chemometrics for saffron authentication and adulteration detection. *Food Chem.* **2021**, *344*, 128647.
(39) Wang, C. Y.; Tang, L.; Jiang, T.; Zhou, Q.; Li, J.; Wang, Y. Z.; Kong, C. H. Geographical traceability of *Eucommia ulmoides* leaves using attenuated total reflection Fourier transform infrared and ultraviolet-visible spectroscopy combined with chemometrics and data fusion. *Ind. Crop. Prod.* **2021**, *160*, 113090.
(40) Lima, A. B. S. D.; Batista, A. S.; Santos, M. R. C.; Rocha, R. D. S. D.; Silva, M. V. D.; Ferrão, S. P. B.; Almeida, V. V. S. D.; Santos, L. S. Spectroscopy NIR and MIR toward predicting simultaneous phenolic contents and antioxidant in red propolis by multivariate analysis. *Food Chem.* **2022**, *367*, 130744.
(41) Ringnér, M. What is principal component analysis? *Nat. Biotechnol.* **2008**, *26*, 303−304.
(42) Lasch, P.; Noda, I. Two-dimensional correlation spectroscopy (2D-COS) for analysis of spatially resolved vibrational spectra. *Appl. Spectrosc.* **2019**, *73*, 359−379.
(43) Dong, J. E.; Zhang, J.; Li, T.; Wang, Y. Z. The Storage Period Discrimination of Bolete Mushrooms Based on Deep Learning Methods Combined With Two-Dimensional Correlation Spectroscopy and Integrative Two-Dimensional Correlation Spectroscopy. *Front. Microbiol.* **2021**, *12*, 771428.
(44) Li, L.; Li, Z. M.; Wang, Y. Z. A method of two-dimensional correlation spectroscopy combined with residual neural network for comparison and differentiation of medicinal plants raw materials superior to traditional machine learning: a case study on Eucommia ulmoides leaves. *Plant Methods* **2022**, *18*, 102.
(45) Dong, J. E.; Zuo, Z. T.; Zhang, J.; Wang, Y. Z. Geographical discrimination of Boletus edulis using two dimensional correlation spectral or integrative two dimensional correlation spectral image with ResNet. *Food Control* **2021**, *129*, 108132.
(46) Borba, A.; Gómez-Zavaglia, A. Infrared spectroscopy: an underexploited analytical tool for assessing physicochemical properties of food products and processing. *Curr. Opin. Food Sci.* **2023**, *49*, 100953.
(47) Baddini, A. L. D. Q.; Santos, J. L. V. D.; Tavares, R. R.; Paula, L. S. D.; Filho, H. D. C. A.; Freitas, R. P. PLS-DA and data fusion of visible Reflectance, XRF and FTIR spectroscopy in the classification of mixed historical pigments. *Spectrochim. Acta. A* **2022**, *265*, 120384.
(48) Wen, H.; Yang, T. M.; Yang, W. Z.; Yang, M. Q.; Wang, Y. Z.; Zhang, J. Y. Comparison of Metabolites and Species Classification of Thirteen Zingiberaceae Spices Based on GC-MS and Multi-Spectral Fusion Technology. *Foods* **2023**, *12*, 3714.
(49) Su, D.; He, J. J.; Zhou, Y. Z.; Li, Y. L.; Zhou, H. J. Aroma effects of key volatile compounds in Keemun black tea at different grades: HS-SPME-GC-MS, sensory evaluation, and chemometrics. *Food Chem.* **2022**, *373*, 131587.
(50) Mei, S. U.; Chen, X. M. Combination of HPLC-orbitrap-MS/MS and network pharmacology to identify the anti-inflammatory phytochemicals in the coffee leaf extracts. *Food Front.* **2023**, *4*, 1395−1412.
(51) Deng, X. D.; Liang, Y. H.; Hu, J. M.; Yang, Y. H. Studies on the mechanism of Gegen Qinlian decoction in treating diabetes mellitus based on network pharmacology. *Nat. Prod. Commun.* **2021**, *16*, 1934578X2098213.
(52) Park, J. Y.; Ahn, E.; Hwang, M. H.; Park, Y. J.; Cho, Y.; Ko, H.; Jeong, W.; Yang, S. H.; Seo, D.; Oh, J. S. Improvement of obesity and dyslipidemic activity of *Amomum tsao-ko* in C57BL/6 mice fed a high-carbohydrate diet. *Molecules* **2021**, *26*, 1638.
(53) Shim, K. S.; Hwang, Y. H.; Jang, S. A.; Kim, T.; Ha, H. Ethanol extract of *Amomum tsao-ko* ameliorates ovariectomy-induced trabecular loss and fat accumulation. *Molecules* **2021**, *26*, 784.
(54) Hong, S. S.; Choi, C. W.; Lee, J. E.; Jung, Y. W.; Lee, J. A.; Jeong, W.; Choi, Y.; Cha, H.; Ahn, E.; Oh, J. S. Bioassay-guided isolation and identification of anti-obesity phytochemicals from fruits of *Amomum tsao-ko*. *Appl. Biol. Chem.* **2021**, *64*, 64.
(55) Bhalani, D. V.; Nutan, B.; Kumar, A.; Singh Chandel, A. K. Bioavailability Enhancement Techniques for Poorly Aqueous Soluble Drugs and Therapeutics. *Biomedicines* **2022**, *10*, 2055.
(56) Hu, Y.; Lin, Q. Z.; Zhao, H.; Li, X. J.; Sang, S. Y.; McClements, D. J.; Long, J.; Jin, Z. Y.; Wang, J. P.; Qiu, C. Bioaccessibility and bioavailability of phytochemicals: Influencing factors, improvements, and evaluations. *Food Hydrocolloid.* **2023**, *135*, 108165.

https://doi.org/10.1021/acsomega.4c03717
ACS Omega 2024, 9, 29857−29869